Fragmentation Transition for Invasion Percolation in Hydraulic Gradients

Anne Vedvik, Geri Wagner, Unni Oxaal,* Jens Feder, Paul Meakin, and Torstein Jøssang

Department of Physics, University of Oslo, P.O. Box 1048, Blindern, N-0316 Oslo, Norway

(Received 17 December 1997)

Air injected into a two-dimensional porous medium displaced a *flowing* defending fluid. At low flow rates the invading air formed chains of fractal clusters similar to those observed in gradient percolation. The defending fluid was excluded from the invading region and moved around the invading clusters. Above a critical flow rate the invaded region fragmented into a plumelike structure that permitted the defending fluid to flow through the invaded region. Invasion percolation simulations, modified to include fragmentation and pressure gradients due to flow, describe the observations well. [S0031-9007(98)05728-7]

PACS numbers: 47.55.Mh, 47.55.Kf, 64.60.Ak

Displacement of one fluid by another is the primary mechanism by which hydrocarbons migrate and are recovered from porous underground reservoirs. Slow immiscible fluid-fluid displacement processes are controlled by capillary forces whereas fast displacements are governed by viscous forces. On long length scales, buoyancy forces due to different fluid densities dominate. The interplay between viscous forces, capillary forces, and buoyancy leads to a variety of fractal displacement front morphologies [1].

Viscous forces may play an important role even in slow displacements [2,3]. If a nonwetting fluid is displacing a *flowing* wetting fluid, the viscous pressure gradient driving wetting fluid affects the displacement process. Such a scenario may be relevant to the secondary migration of hydrocarbon fluid through water-saturated porous rocks (or through fractures), or to the penetration of dense nonaqueous pollutants into water-saturated soils and rocks. In these cases, the flowing water can have a meteoric origin, or the flow may be generated by sediment compaction [4,5].

Here we report an abrupt morphology transition of the displacement front occurring in slow immiscible displacements in the presence of pressure gradients due to flow of the defending fluid. For low pressure gradients, the displacing fluid formed a connected fractal structure with many loops [see Fig. 1(a)], similar to those observed [6,7] in invasion percolation (IP). Defending flowing fluid could not enter such a structure. As the viscous pressure gradient was increased, the structures thinned and elongated along the flow direction. However at high viscous pressure gradients, the invading fluid formed very small fragments distributed over a broad plume shaped region [see Fig. 1(b)]. The displaced defending fluid could freely flow not only around but also through the region containing the invading fluid, although with reduced velocity. The small invading fluid fragments moved by disconnecting and reconnecting, thereby transporting fragments in the direction of pressure gradients created by the flowing defending fluid.

The competition between viscous and capillary forces is described through the dimensionless capillary number $\mathrm{Ca}_w = \mu u a^2/\sigma k$, where μ is the viscosity of the displaced flowing fluid, u is its microscopic pore velocity, a is the size of a typical pore, σ is the interfacial tension, and k is the permeability of the porous medium. Ng *et al.* [8], Morrow [9,10], and Lenormand and Zarcone [11] studied the mobilization of single blobs of nonwetting fluid blobs by flow of surrounding wetting fluid at

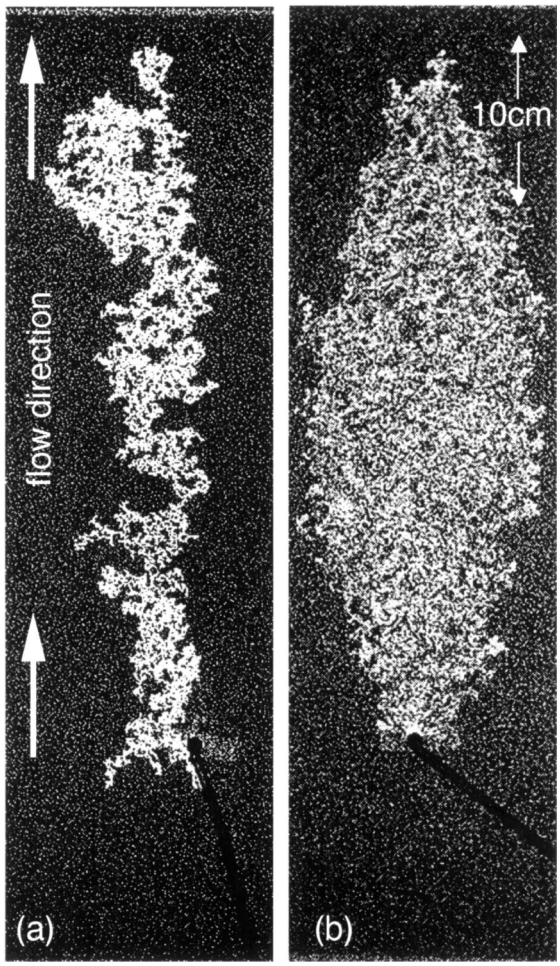

FIG. 1. Patterns obtained by injecting air (white) into a porous medium saturated with water/glycerol (black) flowing upward. (a) $\mathrm{Ca}_w = 15.2 \times 10^{-3}$; (b) $\mathrm{Ca}_w = 112 \times 10^{-3}$.

various values of Ca_w. Payatakes [12] considered the dynamics of a population of blobs of oil trapped in a water-saturated porous medium. Hinkley *et al.* [13] performed experiments in which blob migration velocities were measured as a function of Ca_w, blob size, and viscosity ratio. Birovljev [14] explored migration and fragmentation of an air bubble in a porous medium saturated with initially quiescent water that started to flow during the experiment. The conclusion from these studies is that nonwetting fluid blobs and fragments can become either mobilized or stuck in fluid-saturated porous matrices, depending on the blob size, Ca_w, and the viscosity ratio. Blob fragmentation and coalescence were observed but morphology transitions were not detected.

In capillary-dominated displacements of a wetting fluid by a nonwetting fluid, the nonwetting fluid forms self-similar structures that are well described by the invasion percolation model [15,16]. Uniform fields of force, such as buoyancy, induce characteristic length scales upon the structures. Displacement patterns can often be perceived as an assembly of blobs with an overall size of ξ and a self-similar structure on length scales ℓ in the range $a < \ell < \xi$ [17]. Long-range forces such as buoyancy govern the structure of the blob assembly on length scales beyond ξ. If ξ is related to a parameter describing the competition between capillary forces and long-range forces, properties of the displacement pattern such as the mass density m can be expressed in terms of this parameter. In the presence of gravity, competition between capillary forces and buoyancy is described by the dimensionless Bond number $\mathrm{Bo} = \Delta\rho g a^2/\sigma$. Here, $\Delta\rho$ is the density difference between the fluids and g is the acceleration due to gravity. In displacements restricted by capillary forces but supported by buoyancy (destabilized invasion [18–20]), invading nonwetting fluid forms a string of fractal blobs that is oriented along the direction of the hydrostatic pressure gradient. In quasi-two-dimensional porous media, the mass density of the string scales as [7,17]

$$m \sim |\mathrm{Bo}|^{-\nu(D-1)/(\nu+1)} \sim |\mathrm{Bo}|^{-0.51}, \qquad (1)$$

where $D \approx 1.82$ is the fractal dimensionality of IP-like clusters, measured on length scales in the range $a < \ell < \xi$ [6], and $\nu = 4/3$ is the percolation correlation exponent. The scaling exponent $\nu(D-1)/(\nu+1)$ in Eq. (1) is independent of the nature of the long-range force. It is natural to ask whether the relation holds equally for displacements in the presence of viscous pressure gradients, with Ca replacing Bo. In the experiments and simulations reported here, we find that such a relation exists for low values of Ca_w. Above a critical flow rate of the flowing defending fluid, the scaling relation breaks down as plume-like structures are formed in the displacements. Structure widths and mass densities in this regime are limited by system sizes. Structure morphology changes, from fractal blobs assembled to a string to a homogeneous "cloud" of fragments with a stretched-exponential size distribution.

Experiments.—Monolayers of 1 mm diameter glass beads sandwiched between layers of Plexiglas and glass formed quasi-two-dimensional porous models. The models were similar to those described in Ref. [20] but with ducts fitted at the boundaries to allow the defending fluid flowing through the model. Models of dimensions of 42×80 cm had approximately 200×400 pores and had a porosity of $\phi \approx 0.62$ and a permeability of $k = 0.03 \times 10^{-3}$ cm^2. Nonwetting fluid was air, and defending wetting fluid was a dyed water-glycerol mixture with a viscosity $\mu = 8.0 \pm 0.5$ cP and a surface tension of $\sigma = 64$ dyn/cm with respect to air. A peristaltic pump connected to a reservoir drove the water-glycerol mixture at a constant rate through the model, which initially was completely saturated with the mixture. At the highest flow rates of $Q_w \approx 40$ ml/min used, the pressure difference across the model was of the order of 2700 Pa.

Air was continuously injected into the model through an inlet in the center of the model, using a low constant rate of $Q_{nw} = 0.01$ ml/min. In the early stages of an experiment, air formed a connected structure that resembled an IP cluster. At later stages, the pattern was distorted and, in some cases, fragmented. Fresh air advanced episodically from the inlet to the flanks or the tip of the structure. Each experiment was terminated when air reached the boundary of the model. Ca_w was varied from 3.63×10^{-3} to 112×10^{-3}, corresponding to flow rates Q_w in the range 1.3–40 ml/min.

Figure 2(a) shows the overall length l_{nw} of nonwetting fluid structures (in the flow direction) as a function of air volume M_{nw}, measured in two experiments at $Ca_w = 5.86 \times 10^{-3}$ and $Ca_w = 93.16 \times 10^{-3}$, respectively. At low Ca_w, l_{nw} increased stepwise, but linearly with M_{nw} on average. At high Ca_w, a plume-shaped structure was formed when l_{nw} had reached about 1/3 of the length of the porous model. At this point, the rate of increase of length dropped significantly.

In Fig. 2(c), the mass density m of the displacement structures is plotted on a log-log scale as a function of Ca_w. m was measured by averaging the number of pixels representing air in digitized images of the structures. For $Ca_w < 0.05$, the data are consistent with a power law

$$m \sim \mathrm{Ca}_w^{-\chi}, \qquad (2)$$

with $\chi = 0.53 \pm 0.06$, in agreement with the conjecture that viscous pressure gradients and gravitational pressure gradients lead to similar effects.

Simulations.—In the continuum approximation flow in a porous medium is described by Darcy's law $U = -(k/\mu)\nabla P$, where U is the fluid flux and P is the pressure. For incompressible fluids in stationary flow the pressure field satisfies the Laplace equation $\nabla^2 P = 0$. Simulations of the experimental displacement process were carried out on a triangular lattice of bonds representing the porous model fluid volume. The lattice had a rectangular shape and contained approximately 80 000 bonds.

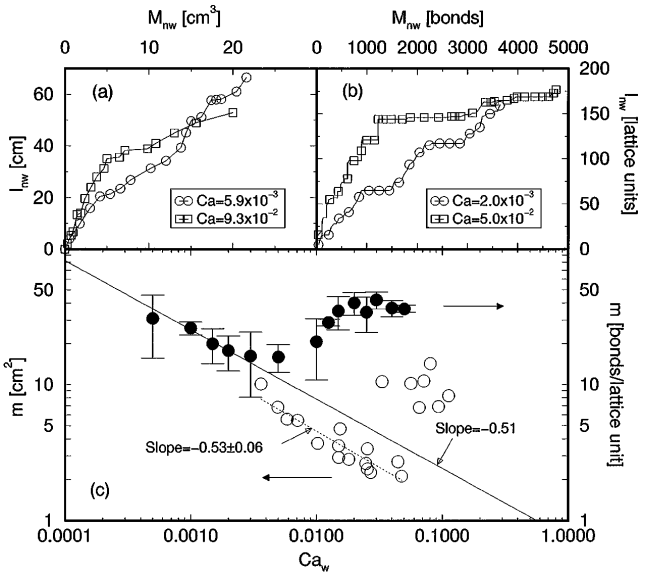

FIG. 2. Parts (a) and (b) show plots of the length l_{nw} of structures of air as a function of the injected air volume M_{nw}, measured in experiments (a) and in simulations (b). Capillary numbers are indicated. Part (c) shows a log-log plot of the linear mass density m as a function of Ca_w, measured at the final stages in the experiments ($\circ$) and in the simulations ($\bullet$). Error bars indicate the standard deviations obtained from averaging the simulation data. For m measured in experimental IP-like structures, a linear least-squares fit was attempted (dotted line). In this regime, experimental data and the simulation data are consistent with theoretical expectations (solid line).

Initially, all bonds were labeled to represent pores filled with wetting fluid, and a random number p_i was assigned to each bond i. These random numbers represented the contribution of capillary forces to the pressure difference across the represented pore if part of the fluid-fluid interface spanned across the pore. A Gaussian distribution of random numbers with a mean value of $\overline{p} = 1.0$ and standard deviation of 0.5 was used in all of the simulations. The wetting fluid was assumed to flow from one end of the lattice to the other, driven by a constant pressure drop ΔP across the system. At each stage in the simulation, the Laplace equation was solved [21] to obtain the viscous pressure field, P, on the lattice nodes that were not adjacent to nonwetting fluid bonds (see Fig. 3). Bond pressures were obtained by interpolation. For bonds inside a fragmented nonwetting fluid structure, P was calculated iteratively, by averaging the pressure at nearest-neighbor bonds with well-defined pressure values. The boundary conditions used were $P = P_0 + \Delta P$ at the inlet, $P = P_0$ at the outlet, and $\mathbf{n} \cdot \nabla P = 0$ at all other boundaries (lattice edges parallel to the flow direction, and interfaces with regions filled with nonwetting fluid), where $\mathbf{n}$ is a unit vector normal to the boundary or interface. Three bonds in the center of the lattice represented the air inlet.

Simulations were based on the IP model with trapping [16] and proceeded via *invasion* and *migration* steps.

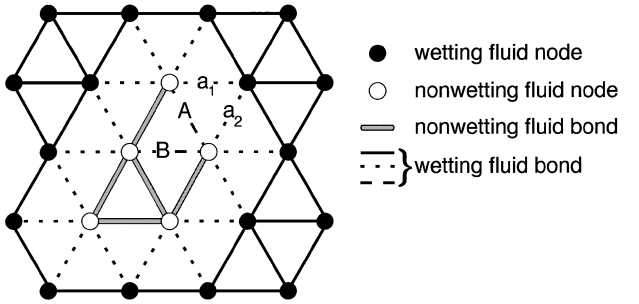

FIG. 3. In simulations the viscous pressure P due to flow of wetting fluid was calculated on wetting fluid nodes in a triangular lattice. For wetting fluid bonds connecting wetting fluid nodes (solid lines), P was interpolated. For wetting fluid bonds connecting a wetting fluid node to a nonwetting fluid node (dotted lines), P was equal to the pressure at the wetting fluid node. For wetting fluid bonds connecting two nonwetting fluid nodes (dashed lines), P was calculated using an iterative procedure. In the example, $P(A) = [P(a_1) + P(a_2)]/2$ and $P(B) = P(A)$.

In each invasion step, nonwetting fluid bonds at the perimeter adjacent to the invaded region that included the inlet were examined. The bond i with the lowest invasion threshold $\pi_i = p_i + P_i$ was invaded, where P_i is the viscous pressure associated to bond i. After each invasion step, migration steps in which nonwetting fluid withdrew from a bond j and invaded another bond i could occur. Migration occurred if the viscous pressure drop was sufficient to drive the invasion of the ith bond,

$$P_j - P_i > p_i \,. \tag{3}$$

Migration could lead to fragmentation of the nonwetting fluidstructure. Among all possible migration steps, the one yielding the highest excess pressure, $P_j - P_i - p_i$, was executed; only migration in the flow direction was allowed. Then $\nabla^2 P = 0$ was solved for the new configuration, and a new migration step was attempted. If, however, the inequality (3) was violated for all bonds then an invasion step was executed.

In simulations, the capillary number Ca_w was given by the mean viscous pressure drop $\overline{\Delta P}$ across a bond, since $\overline{p} = 1.0$. The mass density m was defined as the average number of invaded bonds in rows in the central third of the lattice. At low Ca_w, migration and fragmentation was not possible. At high Ca_w, extensive fragmentation occurred, and plumelike structures were formed, similar to those observed in the experiments. Figure 4 shows two structures obtained at $\mathrm{Ca}_w = 2 \times 10^{-3}$ and $\mathrm{Ca}_w = 5 \times 10^{-2}$, respectively, and Fig. 2(b) shows the dependence of the overall length l_{nw} of these two structures on the "mass" M_{nw} (the number of invaded bonds). The figure is in qualitative agreement with Fig. 2(a). In Fig. 2(c), measurements of m as a function of Ca_w are included. The simulation data compares well to the experimental data, with a scaling regime according to Eq. (1) at low Ca_w, and a roughly constant mass density at high

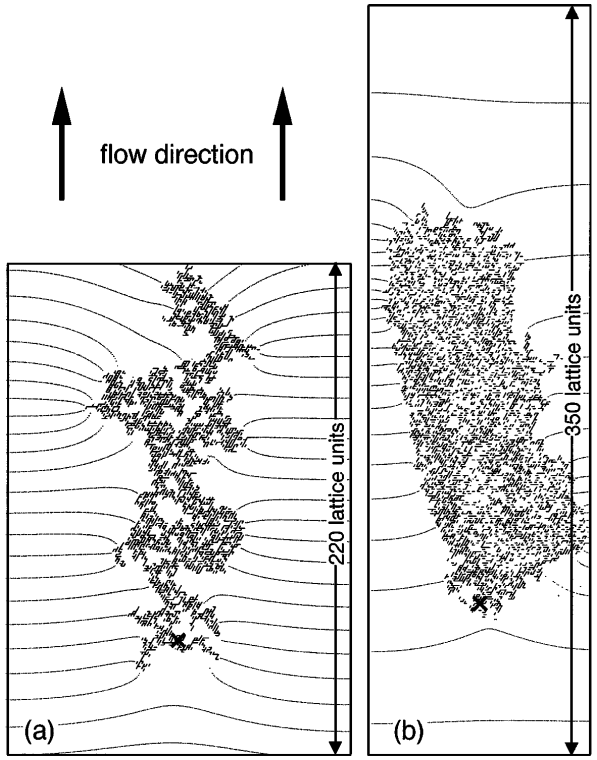

FIG. 4. Patterns obtained in simulations using a modified bond IP model. Part (a) shows a structure observed at $Ca_w = 2 \times 10^{-3}$ on a triangular lattice with 220×128 nodes, and part (b) shows a structure observed at 50×10^{-3} on a 350×88 nodes lattice. Dotted lines represent isopressure curves and a cross indicates the inlet.

Ca_w. The transition occurs at a lower Ca_w than in the experiments. This inconsistency is attributed to the simple way in which the withdrawal of the nonwetting fluid from pores was modeled, ignoring any capillary effects. As in the experiments, the scaling region is limited from above by the morphology transition (at about $Ca_w \approx 10^{-2}$), and from below by finite-size effects.

The effects of gravitational pressure gradients on the invasion percolationlike invasion fronts are fundamentally different from the effects of viscous pressure gradients. Buoyancy is a body force that acts uniformly whereas viscous forces are concentrated onto the most exposed external parts of the air structure. Despite this difference, small viscous pressure gradients were found to affect slow capillary-dominated displacement processes in the same way as hydrostatic pressure gradients.

The fragmentation transition observed in experiments and simulations at high viscous pressure gradients is connected to rupturing of the nonwetting fluid structures. Rupturing led to changes in the flow pattern of the defending water-glycerol mixture, and hence to changes in the viscous pressure field. At low and intermediate Ca_w, rupturing occurred occasionally, but viscous pressure changes were insignificant, compared to (stationary) capillary forces. At high Ca_w, rupturing generated immobile air fragments and caused significant local changes of P. If changes were sufficient to cause migrating air to circumvent the obstacles, even at the price of passing less permeable regions (high capillary forces), the air structure broadened. In contrast, in the presence of body forces such as gravity, obstacles cannot distort the pressure field, and no morphology transition is observed.

We gratefully acknowledge the financial support of the Norwegian Research Council, and VISTA, a research collaboration between Den norske stats oljeselskap, (Statoil) and the Norwegian Academy of Sciences and Letters.

*Present address: Department of Agricultural Engineering, Agricultural University of Norway, P.O. Box 5065, N-1432 Ås, Norway.

[1] R. Lenormand, E. Touboul, and C. Zarcone, J. Fluid Mech. **189**, 165 (1988).
[2] M. M. Dias and A. C. Payatakes, J. Fluid Mech. **164**, 305 (1986).
[3] O. Vizika, D. Avraam, and A. Payatakes, J. Colloid Interface Sci. **165**, 386 (1994).
[4] J. D. Bredehoeft, R. D. Djevanshir, and K. R. Belitz, AAPG Bull. **72**, 416 (1988).
[5] C. M. Bethke, J. D. Reed, and D. F. Oltz, AAPG Bull. **75**, 924 (1991).
[6] R. Lenormand and C. Zarcone, Phys. Rev. Lett. **54**, 2226 (1985).
[7] V. Frette, J. Feder, T. Jøssang, and P. Meakin, Phys. Rev. Lett. **68**, 3164 (1992).
[8] K. M. Ng, H. T. Davis, and L. E. Scriven, Chem. Eng. Sci. **33**, 1009 (1977).
[9] N. R. Morrow, J. Can. Pet. Technol. **18**, 35 (1979).
[10] N. R. Morrow and B. Songkran, in *Proceedings of the Symposium on Surface Phenomena in Enhanced Oil Recovery, Stockholm, Sweden, 1979*, edited by D. O. Shah (Plenum Press, New York, 1981), pp. 387–411.
[11] R. Lenormand and C. Zarcone, Society of Petroleum Engineers of AIME Report No. SPE/DOE 14882, 1986, p. 23.
[12] A. C. Payatakes, Annu. Rev. Fluid Mech. **14**, 365 (1982).
[13] R. E. Hinkley, M. M. Dias, and A. C. Payatakes, Physico-Chem. Hydrodyn. **8**, 185 (1987).
[14] A. Birovljev, Ph.D. thesis, University of Oslo, Norway, 1994.
[15] R. Lenormand and S. Bories, C.R. Acad. Sci. Paris **291**, 279 (1980).
[16] D. Wilkinson and J. F. Willemsen, J. Phys. A **16**, 3365 (1983).
[17] P. Meakin, J. Feder, V. Frette, and T. Jøssang, Phys. Rev. A **46**, 3357 (1992).
[18] C. Jacquin, C.R. Acad. Sci. Paris **300**, 721 (1985).
[19] J. P. Hulin *et al.*, Phys. Rev. Lett. **61**, 333 (1988).
[20] A. Birovljev *et al.*, Phys. Rev. Lett. **67**, 584 (1991).
[21] W. H. Press, B. P. Flannery, S. A. Teukolsky, and W. T. Vetterling, *Numerical Recipes. The Art of Scientific Computing* (Cambridge University Press, Cambridge, England, 1986).